King Saud University

Arabian Journal of Chemistry

www.ksu.edu.sa
www.sciencedirect.com

ORIGINAL ARTICLE

Amendment of palladium nanocubes with iron oxide nanowires for boosted formic acid electro−oxidation

Heba H. Farrag [a], Islam M. Al-Akraa [b],*, Nageh K. Allam [c],
Ahmad M. Mohammad [a],*

[a] *Department of Chemistry, Faculty of Science, Cairo University, Cairo 12613, Egypt*
[b] *Department of Chemical Engineering, Faculty of Engineering, The British University in Egypt, Cairo 11837, Egypt*
[c] *Energy Materials Laboratory, School of Sciences and Engineering, American University in Cairo, New Cairo 11835, Egypt*

Abstract To quickly move the formic acid (FA) fuel cells closer to a real commercialization, an inexpensive, efficient, and durable electrocatalyst for the direct FA electro-oxidation (FAEO) was developed. This involved a sequential modification of a glassy carbon (GC) substrate with palladium nanocubes (ca. 70 nm, nano-Pd) and iron oxide nanowires (nano-FeO$_x$, ca. 40 nm and 150 nm in average diameter and length, respectively). The deposition sequence and loading level of nano-FeO$_x$ in the catalyst were optimized to minimize the catalyst's poisoning with CO that might probably release from a parallel dehydration of FA or from CO$_2$ reduction. Surprisingly, the FeO$_x$/Pd/GC catalyst exhibited a high (21.6 mA cm^{-2}) specific activity for FAEO, which denoted ca. 7 times that of the "pristine" Pd/GC catalyst. This was synchronized with a better (up to fivefold increase in turnover frequency) "long-termed" stability that extended for 90 min of continuous electrolysis at room temperature. A successful effort was dedicated to improving more the catalyst's stability by activating the catalyst electrochemically at –0.5 V vs Ag/AgCl/ KCl (sat.) in 0.2 mol L^{-1} NaOH. The CO stripping agreed perfectly with the impedance analysis in appending the observed enhancement in the catalytic efficiency of FAEO to a favorable electronic modulation at the Pd surface that boosted the oxidative desorption of poisoning CO species at a lower potential.

* Corresponding authors.
  E-mail addresses: islam.ahmed@bue.edu.eg (I.M. Al-Akraa), ammohammad@cu.edu.eg (A.M. Mohammad).

Production and hosting by Elsevier

1. Introduction

Securing the society with energy, water, food, and drugs (EWFD), in order to fulfill the global goals of sustainability, has become essential not only under normal conditions but also during pandemics and disasters. However, unfortunately, receding resources with the increased demand associated with the change in human demographics, land use, and climate change have impeded the achievement of these goals. In the energy sector, the sole dependence on traditional combustion schemes utilizing fossil fuels must be replaced with cleaner renewable technologies (Carmo et al., 2013, Nishimura et al., 2014). One of these green technologies depends on the solar production of hydrogen from water splitters. Hydrogen is then used directly as in electric vehicles or saved to produce electricity via fuel cells (FCs). These FCs look like the regular combustion engines in oxidizing the fuel but they, moreover, feature an enhanced efficiency, durability, reliability, scalability, eco-friendliness, less noisiness, moving flexibility, and easiness of installation which qualified FCs to supply direct power to numerous stationary and portable electronic applications (Braunchweig et al., 2013, Oishi and Savadogo 2013). The fuel cell vehicles (FCVs) received their power from the H_2/O_2 FCs (HFCs) with a power exceeding 140 kW (e.g., Honda Clarity, Toyota Mirai, Hyundai Tucson, etc.) (Eppinger and Huang 2017). Nevertheless, the low (2.2 kW h L^{-1}) volumetric energy densities of H_2, expensive miniaturization of its containers, high energy losses associated with the H_2 compression, liquefaction, and boil-off, and potential risks and challenges associated with its use, storage, and transport have all stimulated a great interest to replace hydrogen with liquid fuels (Egeland-Eriksen et al., 2021).

In this regard, several liquids such as methanol, ethanol, and formic acid (FA) were recommended as low-carbon fuels with favorable convenience in handling and storage. These fuels could simply be obtained from biomass, and they keep high energy densities (up to 1 kW h kg^{-1}) (Mardini and Biçer 2021) and own, moreover, simple structures that simplified their reaction mechanisms and minimized undesired intermediates and byproducts (Zhang 2008). However, comparatively, the ethanol electro−oxidation and the corresponding direct ethanol FCs (DEFCs) received the least attention due to the relatively higher carbon content of ethanol and its complex oxidation mechanism that included several undesired byproducts (Akhairi and Kamarudin 2016). On the other hand, the methanol (MO) and FA electro−oxidations were less complicated with the capability to sustain large volumetric energy densities up to 4820 and 1750 kW h L^{-1}, respectively (Choun 2016).

However, if compared together, the direct formic acid FCs (DFAFCs) appeared more practical than the direct methanol FCs (DMFCs) in terms of safety, efficiency, and fuel/membrane crossover and compatibility (Wang et al., 2004, Al-Akraa et al., 2021). Indeed, the DMFCs suffer from the toxicity, flammability, and high crossover (through Nafion membranes) of methanol together with the slow kinetics of MO. On the other hand, the non-toxicity, volumetric capacity (53 g H_2/L) and low flammability (under ambient conditions) of FA enabled the maturity of the DFAFCs and presaged its use as a H_2 carrier in FCVs with the adaptation of the existing gasoline infrastructure for FA distribution (Eppinger and Huang 2017). Furthermore, FA exhibits much lower crossover (through Nafion membranes) than methanol, perhaps as a result of repulsion between $HCOO^-$ and $-SO_3^-$ groups in the membrane that permits using very thin membranes and highly concentrated fuel solutions in DFAFCs while keeping the loss of open circuit voltage minimum (Yu and Pickup 2008, Zhang et al., 2010, Eppinger and Huang 2017). Last but not least, the theoretical open-circuit potential and energy efficiency (1.40 V, 1.062 %) of the DFAFCs exceed those of the DEFCs (1.145 V, 0.969 %), DMFCs (1.21 V, 0.967 %) and HFCs (1.23 V, 0.830 %) under standard condition (25 °C, 1 atm) (Qian et al., 2006, Zhang 2008).

To commercialize the DFAFCs on a large scale, their overall performance including their power and energy densities, voltage, price, and lifetime have to be optimized. The degradation of the Nafion membrane and the carbon supports has to be resolved, and the water–CO_2 management should be precisely controlled. The electrocatalysis of FAEO denotes a major dilemma as well in justifying the DFAFCs' performance. Since the 1960 s, Pt and Pd represented the most effective catalysts for FAEO (Breiter 1963, Aguilo 1969, El-Deab et al., 2014, El-Nagar et al., 2015, El-Nagar et al., 2017, Asal et al., 2021, Al-Akraa et al., 2022). Other catalysts as gold (Xiang et al., 2001), osmium (Orozco and Gutiérrez 2000), rhodium (Adić and Tripković 1979), and iridium (Ferrer and Victori 1993) were tested but showed much less efficiencies toward FAEO. While employing Pt and Pt-based catalysts for FAEO in DFAFCs was substantial, their high cost, long-term instability, and reduced tolerance against CO poisoning (deactivation) remained challenging (El-Nagar et al., 2014a, 2014b, Al-Akraa and Mohammad 2020). In fact, poisoning the Pt surface originates from the strong adsorption of released intermediates (e.g., CO) during FAEO and this precludes a large Pt area from the participation in the direct FAEO unless a high overpotential is applied.

Comparatively, Pd is less expensive and possesses a much lower tendency for CO poisoning with a better catalytic activity than Pt (Han et al., 2009, Hu et al., 2014, Al-Akraa et al., 2015a, 2015b, 2015c). While several inspections of FAEO on Pd-based surfaces disclaimed the release of CO as a poisoning intermediate (Hu et al., 2012a, 2012b, Zhang et al., 2012, Asal et al., 2022), other reports endorsed its formation in an indirect competing avenue with CO_2 formation (Wang et al., 2014). This poisoning with CO and CO-like intermediates might rationalize the observed gradual deactivation of Pd surfaces in the catalysis of FAEO (Hu et al., 2012a, 2012b, Yuan and Liu 2013). The dissolution of Pd under highly oxidizing conditions would as well contribute to this deactivation (Hu et al., 2012a, 2012b, Yuan and Liu 2013). To ensure a proper functionality for the DFAFCs, the deterioration of their catalytic performance that is inspired by the catalyst's poisoning needs to be overcome. This could happen with a simple amendment or alloying of Pd with other metals (e.g., Au (Liu et al., 2010, Lee et al., 2014), Pt (Jayashree et al., 2005, Al-Akraa et al., 2015a, 2015b, 2015c), Ag (Cui et al., 2014), Ir (Wang et al., 2008, Al-Akraa et al., 2015a, 2015b, 2015c), Ru (Liu et al., 2012), Sn (Liu and Zhang 2009), Cr (Wen et al., 2013), Ni (Shen et al., 2013), Cu (El-Nagar et al., 2014a, 2014b), Co (Wang and Xia 2008), Pb (Li et al., 2010), V (Larsen et al., 2005), Co/Ir (Wang and Xia 2008), Ni/Pt (Sneed et al., 2014), Ni/P (Chang et al., 2014)), with a structural tailoring of Pd to enrich a favorable orientation (Pd (100)) at the surface (Hoshi et al., 2006) or exposing the Pd surface to trace amounts of boosting impurities (Haan et al., 2010). From another perspective, the Pd surfaces refinement with nanostructured transition metal oxides as CoO_x, MnO_x, NiO_x, TiO_x, and FeO_x could enrich the surface with oxygen moiety that boosted the oxidative stripping of poisoning CO at lower overpotentials (Al-Qodami et al., 2018, Elnabawy et al., 2018, Al-Qodami et al., 2022a, Al-Qodami et al., 2022b). The electron vacancy in d-orbitals of these oxides could further accommodate electrons during oxidation to mediate and speed up the kinetics of the reaction (Jin et al., 2022). We, herein, report on the promising electrocatalysis of FAEO on the FeO_x/Pd/GC catalyst whereby Pd nanoparticles (nano-Pd) were directly deposited onto a glassy carbon (GC) substrate before a modification with peerless inexpensive and earth-abundant iron oxide nanowires (nano-FeO_x).

2. Experimental

All reagents were of analytical grades and employed as received. Iron (II) sulfate heptahydrate ($FeSO_4 \cdot 7H_2O$) was purchased from Riedel-de Haën, sulfuric acid and sodium hydroxide pellets were purchased from Sigma-Aldrich. A

glassy carbon (GC, 3.0 mm in diameter with a geometric area of 0.071 cm^2) electrode was used as working electrode after mechanical polishing with emery paper followed by aqueous slurries of finer alumina powder on a cleaning microcloth. An Ag/AgCl/KCl (sat.) and spiral Pt wire were used as reference and counter electrodes, respectively. All potentials in this investigation were measured with respect to the Ag/AgCl/KCl (sat.) reference electrode.

The electrodeposition of nano-Pd onto the bare GC and FeOx/GC electrodes were carried out in 0.1 mol L^{-1} H_2SO_4 electrolyte containing 1.0 mmol L^{-1} $PdCl_2$ at a constant potential electrolysis of 0 V for 300 s. Whereas nano-FeO_x was deposited electrochemically on the GC and Pd/GC electrodes from 0.02 mol L^{-1} $FeSO_4 \cdot 7H_2O$ electrolyte using cyclic voltammetry (CV) between −0.855 V and −1.205 V at 50 mV s^{-1} (Al-Qodami et al., 2018, Al-Qodami et al., 2022a, Al-Qodami et al., 2022b). The impact of nano-FeO_x loading to the Pd/GC catalyst on the catalysis of FAEO was analyzed by depositing nano-FeO_x with variable potential cycles. The anodic activation of the FeO_x/Pd/GC catalyst was achieved at −0.5 V for 10 min in 0.2 mol L^{-1} NaOH electrolyte before electrochemical measurements to enrich the catalyst's surface with highly oxidized states of iron specious which can presumably boost the catalyst's performance toward FAEO.

All the electrochemical and electrocatalytic measurements were performed in a two compartment three-electrode conventional glass cell at a room temperature (∼25 °C) using an EG&G scanning potentiostat (model 273A) operated with Echem 270 software. The current densities were calculated according to the real surface area of the working electrode (to be calculated based on the charge consumed during the hydrogen desorption using a standard value of 0.21 mC cm^{-2}) (Al-Akraa et al., 2015a, 2015b, 2015c). The electrocatalytic activity of the prepared catalysts toward FAEO was measured in 0.3 mol L^{-1} formic acid (FA) solution (pH 3.5) by CV and linear sweep voltammetry (LSV) at scan rate of 100 mV s^{-1}. The pH was adjusted at 3.5 (by adding appropriate amount of NaOH) to ionize appropriate amount (about one third) of formic acid to formate anion which reduces the polarization resistance and enhance the ionic conductivity of the electrolyte (El-Nagar et al., 2013). The CO stripping voltammetry and the electrochemical impedance spectroscopy were measured at open circuit potential in 0.5 mol L^{-1} H_2SO_4 and 0.3 mol L^{-1} formic acid solution (pH 3.5), respectively.

The surface morphology and the elemental composition of the prepared catalysts were examined using a Zeiss Ultra 60 field emission scanning electron microscope (FE-SEM) and energy-dispersive X-ray spectroscopy (EDX, equipped to the Zeiss FE-SEM), respectively. The crystal structure of the catalysts was identified using X-ray diffractometer (XRD, PANalytical, Empyrean) operated with Cu target (λ = 1.54 Å) in the range of 2θ = 20 −100°. The surface chemical analysis of the best catalyst was evaluated using a "Thermo Scientific™ K-Alpha™ X-ray Photoelectron Spectrometer" (XPS, Thermo Fisher Scientific, USA) that operated with a monochromatic microfocused X ray Al K-alpha radiation (10 to 1350 eV) and spot size of 400 mm at a pressure of 109 mbar with a spectrum pass energy of 200 eV and at a narrow spectrum of 50 eV.

3. Results and discussion

3.1. Electrochemical characterization

3.1.1. Effect of deposition order

Cyclic voltammetry (CV) is a powerful tool for following the kinetics of electrochemical reactions with a precise capability for identifying and assessing very minor electroactive species (Al-Akraa et al., 2013). Fig. 1A shows CVs of the Pd/GC, Pd/FeO$_x$/GC and FeO$_x$/Pd/GC catalysts in 0.5 mol L^{-1} H_2SO_4. The Pd/GC catalyst displays the identical characterization of a clean Pd substrate with the surface oxidation extending from 500 to 1200 mV with a subsequent reduction at ca. 450 mV. This was coupled with the hydrogen adsorption/desorption ($H_{ads/des}$) peaks which appeared in the potential range from 0.0 to −200 mV (Al-Akraa et al., 2015). Similar behaviors were observed at the Pd/FeO$_x$/GC and FeO$_x$/Pd/ GC catalysts but the intensities of the PdO reduction peak (at ca. 450 mV) were shorter; informing about the relative decrease in the real surface area of Pd. This was also acceptable in view of the different loaded amounts and/or the partial consumption of the Pd surface in the deposition of nano-FeO_x. The FeO$_x$/Pd/GC catalyst displayed a short redox peak couple at 450 mV and 80 mV that corresponded to the Fe^{2+}/Fe^{3+} transformation (Al-Qodami et al., 2018). The weakness of this peak couple agreed with the instabilities of nano-FeO_x in acidic media (Fu et al., 2021). Alternatively, the CVs of the same set (Pd/ GC, FeO$_x$/GC, Pd/FeO$_x$/GC and FeO$_x$/Pd/GC) of catalysts were recorded in 0.5 mol L^{-1} KOH (Fig. 1B). Similar behaviors for the Pd surface as those in Fig. 1A appeared in 0.5 mol L^{-1} KOH (Fig. 1B) but at different potentials; the Pd oxidation at (−100 to 600 mV), the PdO reduction at (ca. −400 mV) and the $H_{ads/des}$ at (orange circles, ca. −850 mV for desorption and less than −1.0 V for adsorption). In addition, a new redox peak (blue circles, oxidation at −640 mV and reduction at −850 mV) appeared for nano-FeO_x which corresponded to the reversible Fe(II)/Fe(III) oxide transformation (Doyle and Lyons 2013). Existence of nano-FeO_x in FeO$_x$/Pd/GC catalyst improved largely the $H_{ads/des}$; as indicated at ca. −850 mV (Faid et al., 2019).

3.1.2. Effect of nano-FeO$_x$ loading

The loading of nano-FeO_x in the FeO$_x$/Pd/GC catalyst was optimized for FAEO. Fig. 2A and B show the characteristic CVs in acidic and alkaline media, respectively, of the Pd/GC catalyst and several FeO$_x$/Pd/GC catalysts of variable nano-FeO$_x$ loading (the loading was varied by increasing the deposition cycles, N). Fig. 2A shows a drop in the intensities of the PdO reduction peak and the H_{des} peak in 0.5 M H_2SO_4 with the nano-FeO_x loading. The same behavior was repeated in 0.5 mol L^{-1} KOH (Fig. 2B); concurrently with a gradual rise in the intensity of the redox peak couple (observed from ca. −800 mV to −600 mV). As obviously seen, the peak potential for PdO reduction was shifted to lower overpotentials at the nano-FeO$_x$-modified catalysts if compared to the Pd/GC catalyst; recommending a vital moderation in the electronic properties of Pd at the catalyst' surface. Needless to indicate that the surface coverage of Pd decreased significantly with the loading of nano-FeO_x. It is also easy to notice the unique characteristics for the FeO$_x$/Pd/GC catalyst that was loaded with nano-FeO_x for 4 cycles. This included the highest negative shift in the peak
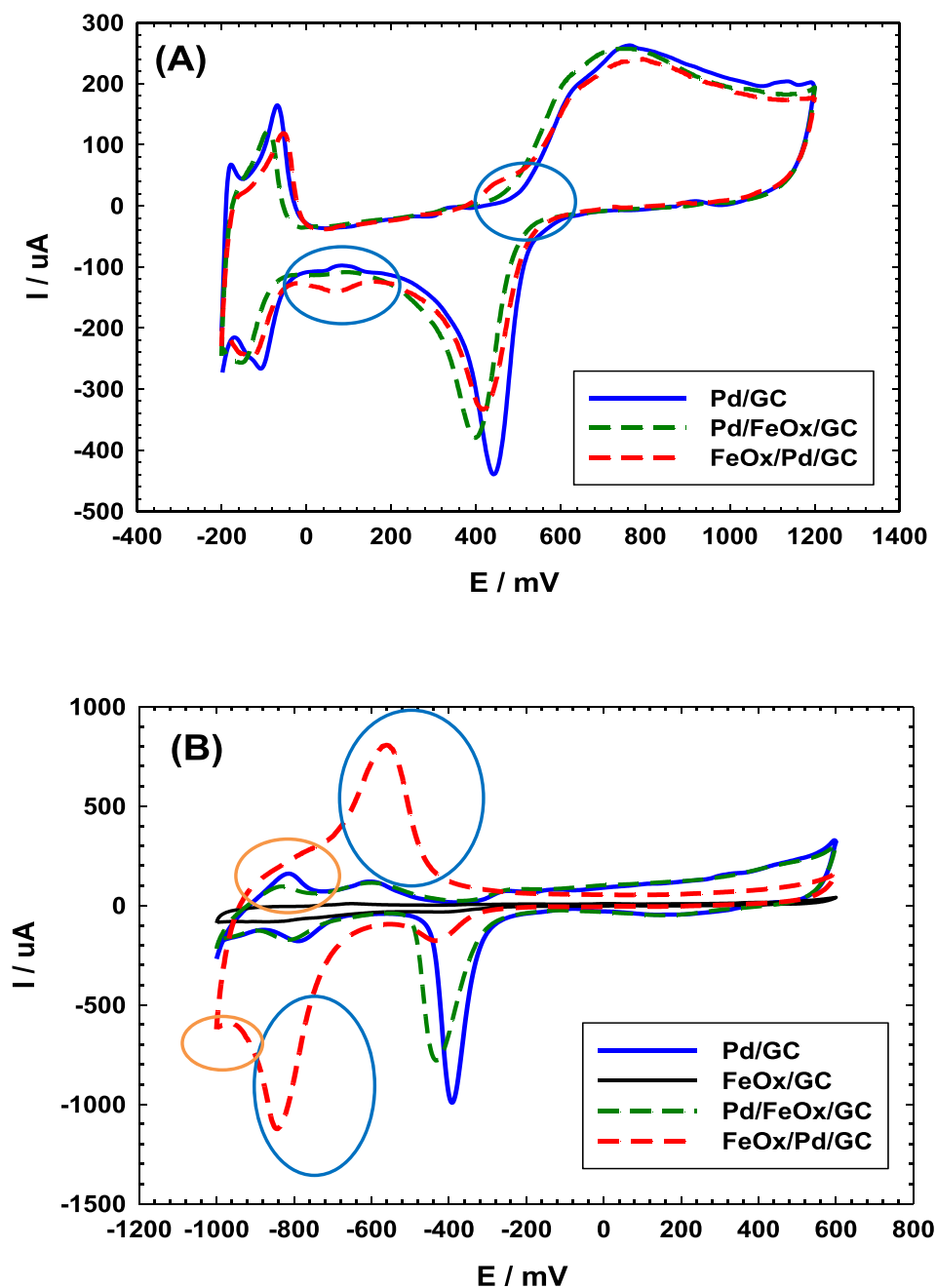
Fig. 1 CVs obtained at "pristine" and FeO_x-modified GC electrodes in (A) 0.5 M H_2SO_4 and (B) 0.5 M KOH (4 potential cycles were applied for the deposition of nano-FeO_x).

potential of PdO reduction (almost similar to the case of 2 cycles deposition of nano-FeO_x), in addition to the obvious detection (higher intensities) of Fe(II)/Fe(III) oxide transformation (at ca. 480 mV in the anodic scan and ca. 80 mV in the cathodic scan, Fig. 2A). The same Fe(II)/Fe(III) oxide transformations appeared at lower overpotentials in an alkaline medium (Fig. 2B).

3.1.3. Effect of activation

Moreover, an anodic activation of the FeO_x/Pd/GC was carried out at –0.5 V to enrich the catalyst's surface principally in the oxide form. Fig. 3 shows the characteristic CVs of FeO_x/

Pd/GC before and after activation. In Fig. 3A, the intensity of the PdO reduction peak increased after activation which recommended a significant dissolution of nano-FeO_x during the activation. A similar behavior was observed in an alkaline medium (Fig. 3B).
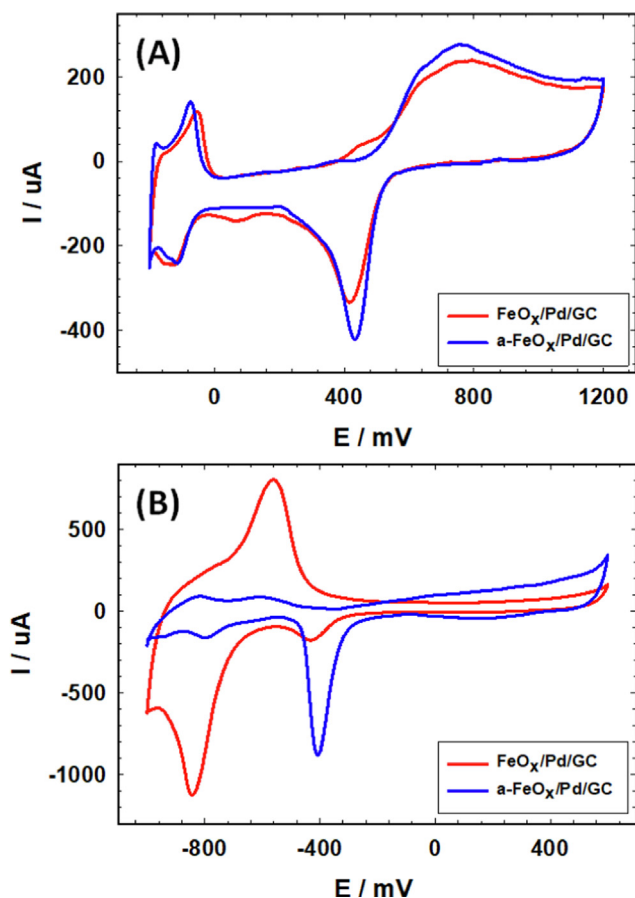
3.2. Material's characterization

Fig. 4 represents the FE-SEM surface morphologies of the Pd/GC, FeO_x/GC, a-FeO_x/GC, Pd/FeO_x/GC, FeO_x/Pd/GC and a-FeO_x/Pd/GC catalysts. The Pd/GC catalyst (Fig. 4A) indicated the deposition of Pd in nanocubes of an average edge size
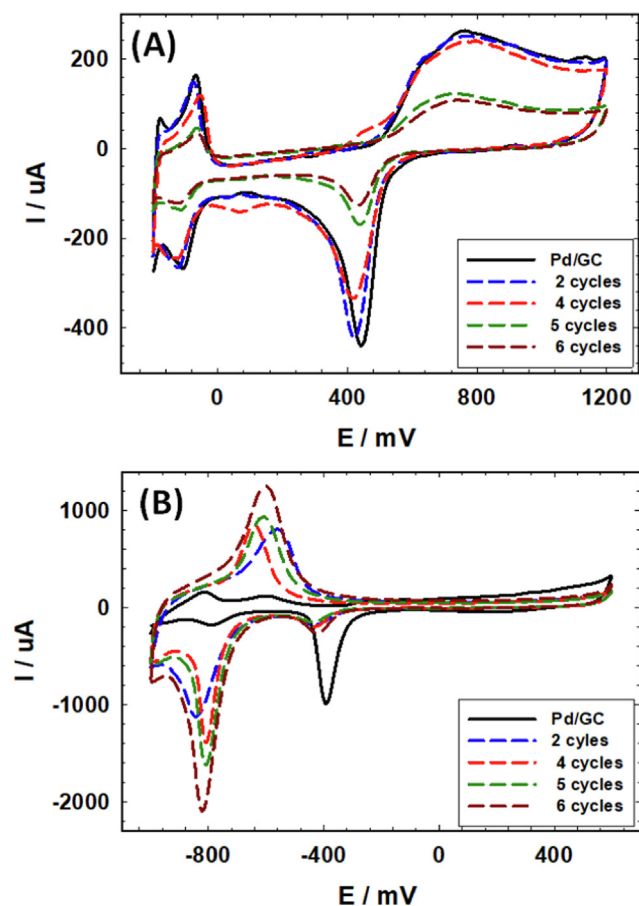
Fig. 2 CVs obtained in (A) 0.5 M H_2SO_4 and (B) 0.5 M KOH at the unmodified Pd/GC (solid black line) and FeO_x-modified Pd/GC (dashed lines) catalysts with various loadings of nano-FeO_x (Legend indicates the no. of cycles involved in the deposition of nano-FeO_x).

Fig. 3 CVs obtained at the inactivated FeO_x/Pd/GC and activated a-FeO_x/Pd/GC catalysts in (A) 0.5 M H_2SO_4 and (B) 0.5 M KOH (4 potential cycles were applied for the deposition of nano-FeO_x).

of ca. 70 nm. Whereas the FeO_x/GC catalyst (Fig. 4B) indicated the deposition of nano-FeO_x mostly as individual intersected nanowires (ca. 40 nm in diameter and 150 nm in length). These nanowires appeared clustered intensively (white aggregates) in several areas. The catalyst's activation (a-FeO_x/GC catalyst, Fig. 4C) did not change the nanowire texture but rather enhanced the fusion of aggregated particles. This denied the conceptional view of being nano-FeO_x dissolved completely during activation. For the Pd/FeO_x/GC catalyst (Fig. 4D), nano-Pd (ca. 90 nm) appeared relatively larger than in the Pd/GC catalyst (Fig. 4A) which agreed perfectly with the data in Fig. 1 (larger surface area of Pd in the Pd/FeO_x/GC catalyst). Interestingly, when nano-FeO_x was deposited onto the Pd/GC surface, the agglomeration of nano-FeO_x disappeared significantly (Fig. 4E) but returned back after activation in a well-defined nanowire structured assembly (Fig. 4F). The exposure of the underneath Pd and GC surfaces were obvious in Fig. 4 E-F, which predicts the participation of nano-Pd in the catalysis of FAEO.

The elemental compositions of the catalysts were evaluated from the EDX analyses (Fig. 5). The relative compositions of the catalytic constituents of all catalysts are given in Table 1. The EDX measurements revealed the effective electrodeposi-

tion of Pd (43.90 wt%) and Fe (90.82 wt%) onto the Pd/GC and FeO_x/GC electrodes, resepctively. The activation at – 0.5 V led to reducing the amount of Fe (78.30 wt%) with the increase of oxygen content which accounted on the further oxidation and the possible dissolution of Fe. Data for the successive deposition of both metals on the GC substrate are shown in Fig. 5 and Table 1. For the Pd/FeO_x/GC catalyst, the EDX spectrum could not detect Fe perhaps due to the complete coverage of Fe with Pd, taking into consideration the limitation of EDX to detect the small amount of Fe at the surface. However, in the case of FeO_x/Pd/GC catalyst, the EDX spectrum detected both Fe (73.55 wt%) and Pd (15.21 wt%) which agreed with the layers' hierarchy.

Furthermore, the crystal structures of the Pd/GC, FeO_x/Pd/GC and a-FeO_x/Pd/GC catalysts were examined with the XRD technique (Fig. 6A). Fig. 6A (a) shows several diffraction peaks for the Pd/GC catalyst at ca. 25°, 39°, 43°, 64° and 78° corresponding, respectively, to the (0 0 2) plane of C (JCPDS card No. 075–1621) (Asal et al., 2022), (1 1 1), (2 0 0), (2 2 0) and (3 1 1) planes of Pd (JCPDS card No. 96–101-1105) (Asal et al., 2022) that reflected its face-centered cubic (fcc) structure (Al-Akraa et al., 2015). The XRD spectra of FeO_x/Pd/GC and a-FeO_x/Pd/GC (Fig. 6A (b and c)) showed no clear difference compared to the Pd/GC catalyst; recommending the retention of the same crystal structure of nano-
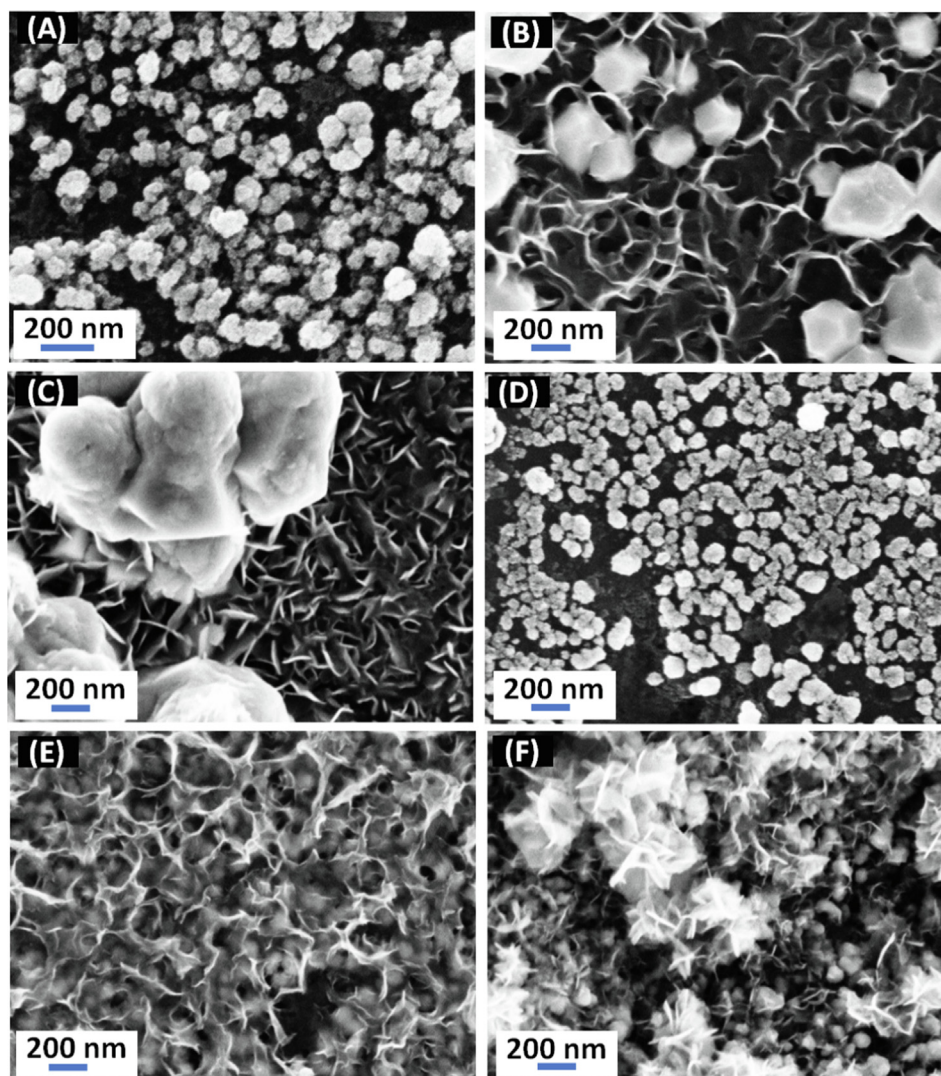
Fig. 4 FE-SEM (high magnification) images for (A) Pd/GC, (B) FeO$_x$/GC, (C) a-FeO$_x$/GC, (D) Pd/FeO$_x$/GC, (E) FeO$_x$/Pd/GC and (F) a-FeO$_x$/Pd/GC catalysts (4 potential cycles were applied for the deposition of nano-FeO$_x$).

Pd in all the catalysts. Unfortunately, the sensitivity of the spectroscope was not sufficient to detect nano-FeO$_x$ which existed at the electrode's surface. However, assembling of nano-FeO$_x$ in the FeO$_x$/Pd/GC catalyst decreased the ratio of diffraction peak intensities of Pd (200): Pd (111) but it increased back after activation. The deposition of nano-FeO$_x$ onto the Pd (200) facet is presumable.

The chemical oxidation states of the elements at the surface of the FeO$_x$/Pd/GC catalyst were estimated by XPS. The Fe 2p peak of the FeO$_x$/Pd/GC catalyst was deconvoluted in two peaks at binding energies of 713.1 and 725.1 eV (Fig. 6B), which were assigned to the 2p$_{3/2}$ and 2p$_{1/2}$ peaks of Fe^{+3} (Al-Qodami et al., 2022a, 2022b). These peaks accompanied two shake-up satellites at 719.7 (Fe 2p$_{3/2}$, sat) and 729.1 (Fe 2p$_{1/2}$, sat) eV resulting from the charge transfer or shake-up processes associated with Fe^{+3}. The peak observed at 710.7 was assigned to Fe^{+2} (Al-Qodami et al., 2022a, 2022b). Fig. 6C shows the Pd 3d spectrum for FeO$_x$/Pd/GC catalyst that was deconvoluted into Pd 3d$_{5/2}$ and Pd 3d$_{3/2}$ at ca. 335 and 341 eV, respectively and assigned to metallic Pd (Maji

et al., 2020). Two other peaks at 336.2 and 342.1 eV were assigned to Pd 3d$_{5/2}$ and Pd 3d$_{3/2}$ of PdO (Maji et al., 2020). These analyses of Pd 3d spectrum confirmed the existence of Pd at the surface in both Pd (0) and Pd (II) species. The O 1s peak in (Fig. 6D) was deconvoluted into three different peaks at ∼ 530, 532, and 534 eV corresponding, respectively, to the lattice oxygen of Fe—O—Fe bonding in FeOOH, lattice oxygen of Fe—O—H bonding in FeOOH and oxygen in the H—O—H bonding of chemisorbed water at the FeOOH surface (Al-Qodami et al., 2022a, 2022b). The presence of chemisorbed water confirmed the hydrated nature of nano-FeO$_x$ at the catalyst surface.

3.3. Formic acid electro-oxidation (FAEO):

3.3.1. Effect of deposition sequence

Fig. 7 shows the CVs of FAEO at the Pd/GC, Pd/FeO$_x$/GC and FeO$_x$/Pd/GC catalysts in 0.3 M FA (pH 3.5). In fact, the unmodified GC and the FeO$_x$/GC catalysts did not show any electrocatalytic activity toward FAEO as was reported
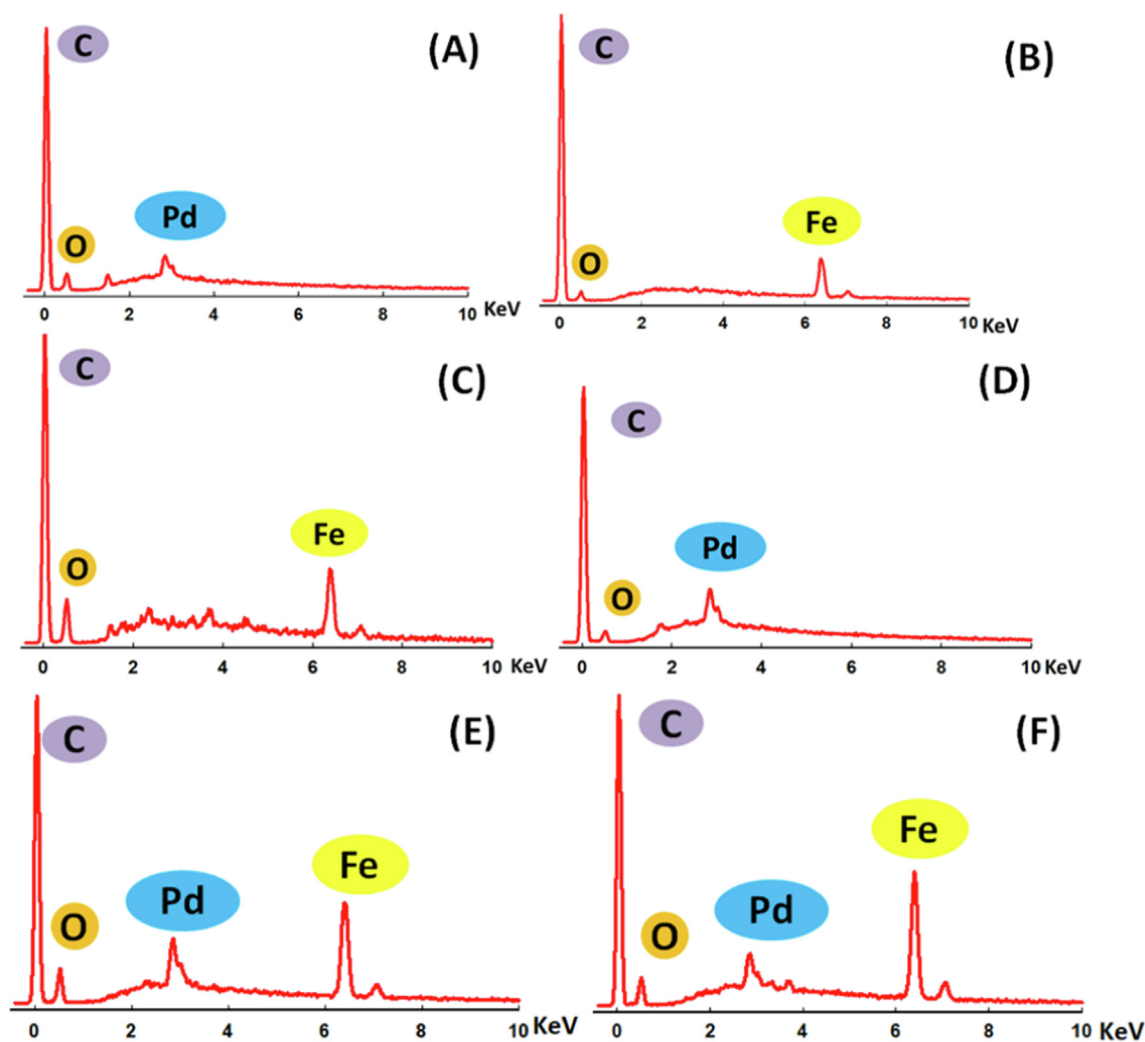
Fig. 5 EDX spectra of (A) Pd/GC, (B) FeO$_x$/GC, (C) a-FeO$_x$/GC, (D) Pd/FeO$_x$/GC, (E) FeO$_x$/Pd/GC and (F) a-FeO$_x$/Pd/GC catalysts (4 potential cycles were applied for the deposition of nano-FeO$_x$).

Table 1 Elemental compositions of catalysts as revealed from EDX measurements.

Catalyst	Pd (mass %)	Fe (mass %)	O (mass %)
Pd/GC	43.90	0	56.10
FeO$_x$/GC	0	90.82	9.18
a-FeO$_x$/GC	0	78.30	21.70
Pd/FeO$_x$/GC	59.41	0	40.59
FeO$_x$/Pd/GC	15.21	73.55	11.24
a-FeO$_x$/Pd/GC	22.03	60.89	17.08

earlier (Al-Qodami et al., 2018). Fig. 7 revealed that the reaction pathway of FAEO on all (Pd/GC, Pd/FeO$_x$/GC and FeO$_x$/Pd/GC) catalysts proceeded exclusively via the dehydrogenation pathway that produced directly CO$_2$ at ca. 100 mV. Nothing indicated the operation of the "dehydration" pathway that releases the poisoning CO as an intermediate (Baik et al., 2011, Al-Akraa et al., 2015). The intensity of the peak current density (i$_p$) of FAEO was taken as an index to probe the activity of the catalysts. The relative increase (2 times that of the Pd/GC catalyst) in the i$_p$ of the Pd/FeO$_x$/GC catalyst

interpreted the role of nano-FeO$_x$ in orienting the deposition of nano-Pd in preferable facets for FAEO. Interestingly, the FeO$_x$/Pd/GC catalyst exhibited a sevenfold increase in i$_p$ (in relative to that of the Pd/GC catalyst) that turned this structural hierarchy of this catalyst desirable. Interestingly, the activity of FeO$_x$/Pd/GC catalyst toward FAEO bettered to a great extent many other catalysts in literature, as indicated in Table 2 (Al-Akraa et al., 2015a, Al-Akraa et al., 2015b, Al-Akraa et al., 2015c).

3.3.2. Effect of nano-FeO$_x$ loading

Furthermore, Fig. 8 shows the linear sweep voltammetry (LSV) of FAEO obtained at the Pd/GC and FeO$_x$/Pd/GC catalysts (nano-FeO$_x$ was deposited for various deposition cycles). Obviously, four cycles of nano-FeO$_x$ deposition onto the Pd/GC catalyst exhibited the highest i$_p$. This matched the unique characteristic behavior that was observed for the same loading in Fig. 2. In Fig. 2B, the intensity of the reduction peaks of nano-FeO$_x$ (at −800 mV) increased with increasing the number of deposition cycles due to the increase in the amount of nano-FeO$_x$. It was believed that increasing the amount of nano-FeO$_x$ might lead to a catalytically more active
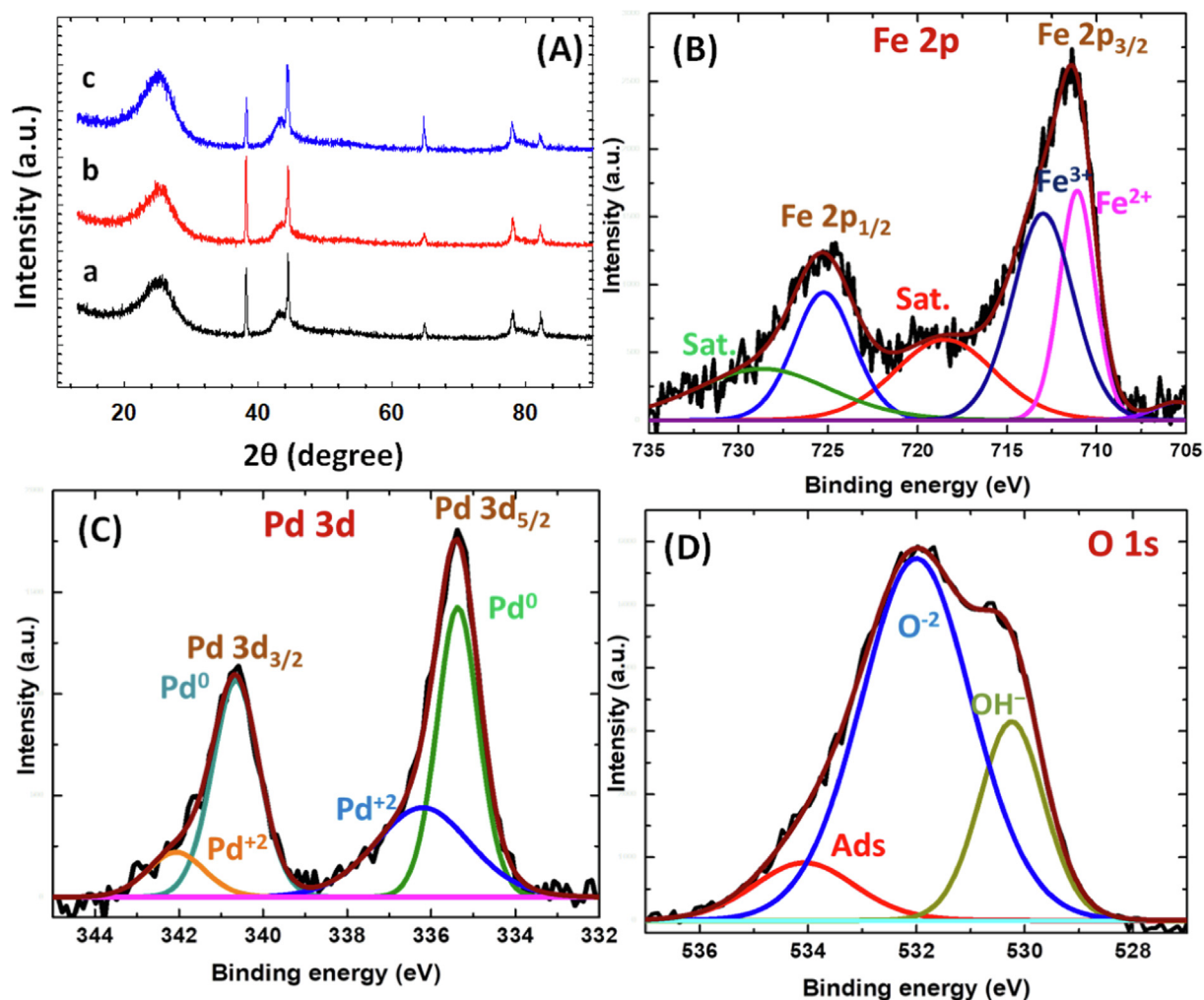
Fig. 6 (A) XRD spectra of (a) Pd/GC, (b) FeO_x/Pd/GC and (c) a-FeO_x/Pd/GC catalysts. (B-D) XPS spectra of Fe 2p (B), Pd 3d (C) and O 1 s (D) peaks of FeO_x/Pd/GC catalyst (4 potential cycles were applied for the deposition of nano-FeO_x).
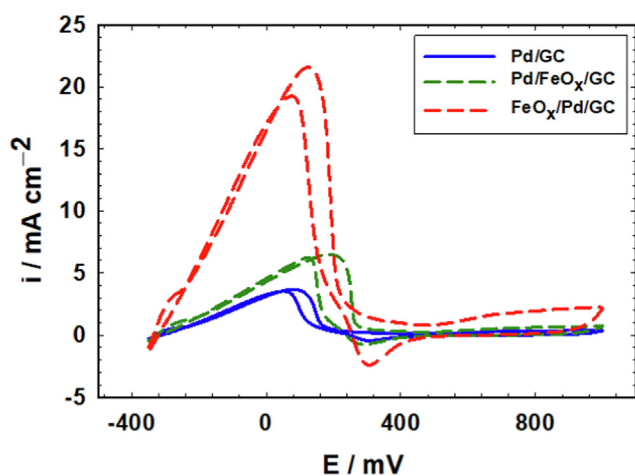

Fig. 7 CVs obtained at Pd/GC, Pd/FeO_x/GC and FeO_x/Pd/GC catalysts in 0.3 M FA (pH 3.5) (4 potential cycles were applied for the deposition of nano-FeO_x).

Table 2 A comparison of the electrocatalytic activities for different catalysts toward FAOR.

Catalyst	i_p / mA cm^{-2}	Ref.
Pd/GC	2.50	Al-Akraa et al., 2015
Pt/Pd/GC	1.23	Al-Akraa et al., 2015
Ir/Pd/GC	6.00	Al-Akraa et al., 2015
NiO_x/Pd/GC	8.00	Al-Akraa et al., 2015
a-FeO_x/Pd/GC	17.5	This work
FeO_x/Pd/GC	21.6	This work

(higher i_p in Fig. 8) surface, which did not happen all the way forward. Indeed, this verified for 2 and 4 cycles but declined for further loadings (5 and 6 cycles) of nano-FeO_x. This can be realized in view of the dependence of the electrocatalytic activity of the FeO_x/Pd/GC on the available surface area of Pd. Therefore, after certain coverage (N = 4) of nano-FeO_x in the FeO_x/Pd/GC catalyst, the decrease in the surface area
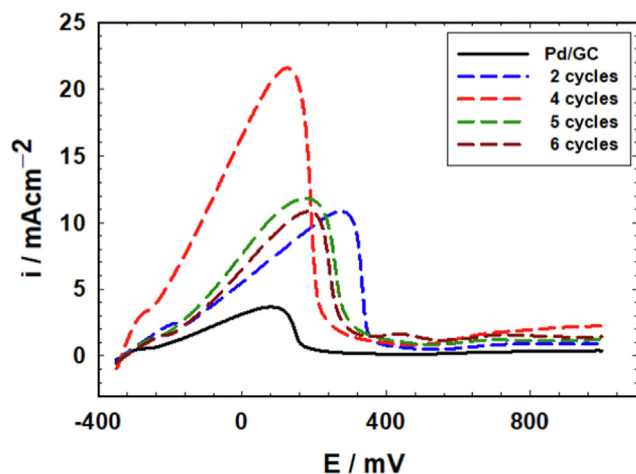
Fig. 8 LSVs obtained in 0.3 M FA (pH 3.5) at the unmodified Pd/GC (solid black line) and FeO_x modified Pd/GC (dashed lines) catalysts (Legend indicates the no. of cycles involved in the deposition of nano-FeO_x).

Fig. 9 CVs obtained at FeO_x/Pd/GC and a-FeO_x/Pd/GC catalysts in 0.3 M FA (pH 3.5) (4 potential cycles were applied for the deposition of nano-FeO_x).

of nano-Pd led to a corresponding decrease in the catalytic activity of the catalyst where the Pd area became limiting for the kinetics of FAEO (El-Nagar et al., 2012). The real surface area (calculated from the charge consumed during the reduction of the Pd oxide surface in 0.5 M H_2SO_4 using a reported value of 420 $\mu C\ cm^{-2}$) and the electrocatalytic activity of all prepared catalysts are summarized in Table 3.
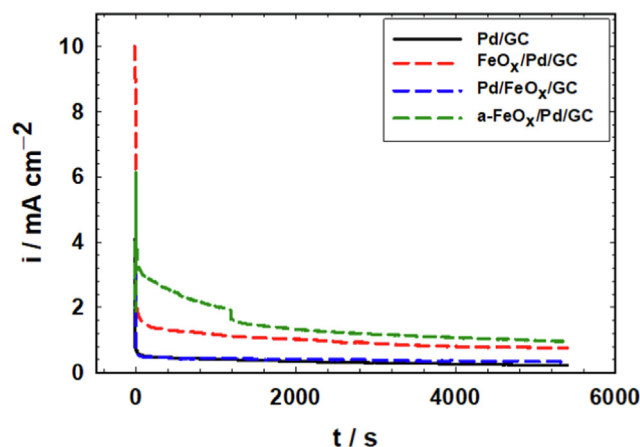
3.3.3. Effect of activation

The effect of activation on the catalysis of FAEO is represented in Fig. 9. The catalytic activity of FAEO did not change much after the activation of the FeO_x/Pd/GC catalyst. The i_p of FAEO decreased from 21.5 mA cm^{-2} (before activation) to 17.5 mA cm^{-2} (after activation). The reason may originate from a partial dissolution of nano-FeO_x after activation as revealed from EDX data (Table 1) that influenced the catalyst's activity.

3.4. Stability toward FAEO

Long-term stabilities of catalysts are essential for a practical application of DFAFCs. Fig. 10 foresees the relative catalysts' stabilities, in which the current transients (i-t) were measured at the Pd/GC, Pd/FeO_x/GC, FeO_x/Pd/GC and a-FeO_x/Pd/GC catalysts in 0.3 M FA (pH 3.5) at 100 mV. It is obvious that the Pd/GC and the Pd/FeO_x/GC catalysts possessed poor
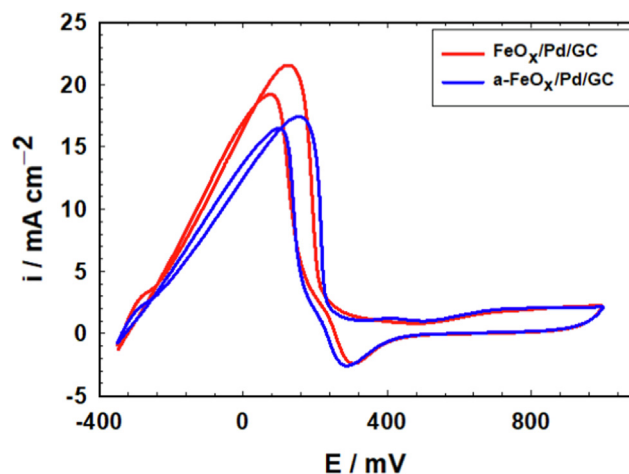
Fig. 10 Current transients (i-t) measured at Pd/GC, Pd/FeO_x/GC, FeO_x/Pd/GC and a-FeO_x/Pd/GC catalysts in 0.3 M FA (pH 3.5) at 100 mV (4 potential cycles were applied for the deposition of nano-FeO_x).

stabilities toward FAEO as reflected from their fast-chronical current decay; in agreements with previous reports (Hong et al., 2011, Al-Akraa et al., 2015). The FeO_x/Pd/GC and a-FeO_x/Pd/GC catalysts exhibited slower current decays and ended up with much better activities (1.0 and 1.2 mA cm^{-2} at the FeO_x/Pd/GC and a-FeO_x/Pd/GC catalysts, respectively). The superiority of the a-FeO_x/Pd/GC in persisting the outmost durability might originate from the conversion of Fe to higher oxides capable to mitigate the possible surface poisoning and/or improve the mechanical properties of the surface film of the catalytic ingredients. Turnover frequencies (TOF) of the catalysts (Table 4) were calculated to assess the intrinsic activity of the catalysts and the efficiency of their active sites (Anantharaj et al., 2021). The better durability and intrinsic activity of the FeO_x/Pd/GC and a-FeO_x/Pd/GC catalysts supported their improved efficiency toward FAEO. This could possibly originate with the electronic amendment that nano-FeO_x made for the electronic properties of Pd at the catalyst's surface against poisoning or dissolution of the

Table 3 The electrocatalytic activities of different catalysts toward FAOR.

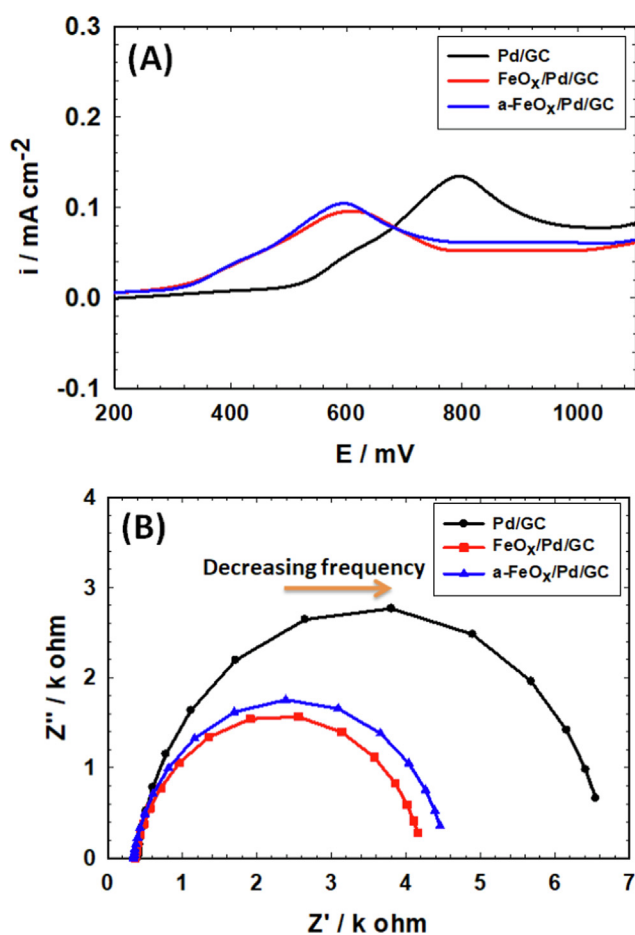| Catalyst	No. of deposition cycles of nano-FeO_x	Real surface area / cm^2	i_p / mA cm^{-2}
Pd/GC	0	0.58	3.66
FeO_x/Pd/GC	2	0.51	11.0
FeO_x/Pd/GC	4	0.42	21.6
FeO_x/Pd/GC	5	0.21	12.0
FeO_x/Pd/GC	6	0.16	10.8
Pd/FeO_x/GC	4	0.57	6.52
a-FeO_x/Pd/GC	4	0.53	17.5

Table 4 Turnover frequency (TOF) of the Pd/GC, Pd/FeO$_x$/GC, FeO$_x$/Pd/GC and a-FeO$_x$/Pd/GC catalysts (4 potential cycles were applied for the deposition of nano-FeO$_x$).

Catalyst	TOF (s^{-1})
Pd/GC	0.113
Pd/FeO$_x$/GC	0.135
FeO$_x$/Pd/GC	0.526
a-FeO$_x$/Pd/GC	0.593

Table 5 Impedance parameters obtained for FAEO at the Pd/GC, FeO$_x$/Pd/GC and a-FeO$_x$/Pd/GC catalysts. The data were obtained from the corresponding EIS spectra (Fig. 11).

Catalyst	R$_s$ [kΩ]	R$_{ct}$ [kΩ]	CPE [μFs$^{(\alpha-1)}$]	α
Pd/GC	0.401	6.301	26.79	0.9195
FeO$_x$/Pd/GC	0.366	4.212	29.73	0.8849
a-FeO$_x$/Pd/GC	0.342	3.872	32.17	0.8724

catalytic ingredients (Hu et al., 2012). Deeper insights for FAEO reaction mechanism at the FeO$_x$/Pd/GC catalyst will soon be investigated.

3.5. Origin of enhancement

To appraise the role of nano-FeO$_x$ in the catalytic improvement toward FAEO, carbon monoxide (CO) stripping voltammetry was carried out at the Pd/GC, FeO$_x$/Pd/GC and a-FeO$_x$/Pd/GC catalysts in 0.5 mol L^{-1} H$_2$SO$_4$ at 50 mV s^{-1} (Fig. 11A) after allowing CO to be adsorbed at the catalysts' surfaces from 0.5 M FA at open circuit potential (OCP) for

15 min. The CO oxidation peak appeared at ca. 0.8 V with a current density of 0.14 mA cm^{-2} at the Pd/GC catalyst. This peak appeared at ca. 0.6 and 0.58 V with ca. 0.097 and 0.107 mA cm^{-2} for the FeO$_x$/Pd/GC and a-FeO$_x$/Pd/GC catalysts, respectively (Fig. 11A). The large negative shift (ca. −200 mV) of the CO oxidation peak potential at the FeO$_x$/Pd/GC and a-FeO$_x$/Pd/GC catalysts strengthened the electronic influence of nano-FeO$_x$ in the catalytic enhancement. The integrated areas below the CO desorption peaks of the FeO$_x$/Pd/GC and a-FeO$_x$/Pd/GC catalysts looked a little smaller than that of the Pd/GC catalyst; recommending a better mitigation of CO poisoning.

The electrochemical impedance spectra (EIS) of the Pd/GC, FeO$_x$/Pd/GC and a-FeO$_x$/Pd/GC catalysts were carried out in 0.3 M FA (pH 3.5) at OCP. The solution resistance (R$_s$), charge transfer resistance (R$_{ct}$) and constant phase element (CPE) of the catalysts were depicted by EIS using Randle's equivalent circuit model (data are listed in Table 5) (Al-Akraa et al., 2017, Ye et al., 2017). The Nyquist plots appeared in Fig. 11B show semicircles with arc diameters that increased in the order of Pd/GC > a-FeO$_x$/Pd/GC > FeO$_x$/Pd/GC catalysts, indicating the lowest R$_{ct}$ for the FeO$_x$/Pd/GC catalyst. On the other hand, the increases in the CPE of the catalysts from Pd/GC, a-FeO$_x$/Pd/GC to FeO$_x$/Pd/GC revealed similar improvement in the number of active sites at the catalysts' surface which led to better catalytic activities (Shervedani and Bagherzadeh 2008).

4. Conclusion

An efficient binary nanocatalyst for FAEO was prepared by a simple modification of the GC catalyst with nano-Pd and nano-FeO$_x$. The deposition sequence of nano-Pd and nano-FeO$_x$ on the GC catalyst and the loading level of nano-FeO$_x$ affected intensively the catalytic activity and stability of the catalyst toward FAEO. The highest catalytic activity (ca. 7 times compared to "pristine" Pd/GC catalyst) was obtained at the FeO$_x$/Pd/GC catalyst (where 4 cycles were employed for the deposition of nano-FeO$_x$ onto the Pd/GC catalyst). The XPS data confirmed the retention of nano-FeO$_x$ at the surface of the FeO$_x$/Pd/GC in two different oxidation states Fe (II, minor) and Fe (III, major). Moreover, the activation of the FeO$_x$/Pd/GC catalyst at –0.5 V improved the catalyst's stability. The CO stripping voltammetry and EIS confirmed the electronic role in the catalytic enhancement.

Declaration of Competing Interest

The authors declare that they have no known competing financial interests or personal relationships that could have appeared to influence the work reported in this paper.

Fig. 11 Oxidative stripping of CO from the Pd/GC, FeO$_x$/Pd/GC and a-FeO$_x$/Pd/GC catalysts in 0.5 M H$_2$SO$_4$ at scan rate 50 mV s^{-1} (A). Nyquist plots (at open circuit potentials) for the same catalysts measured in 0.3 M FA (pH 3.5) (B) (4 potential cycles were applied for the deposition of nano-FeO$_x$).

Data availability

Data will be made available on request.

References

Adić, R.R., Tripković, A.V., 1979. Optical and electrochemical study of electrocatalysis by foreign metal adatoms: Oxidation of formic acid on rhodium. J. Electroanal. Chem. Interfacial Electrochem. 99, 43–53. https://doi.org/10.1016/S0022-0728(79)80409-X.

Aguilo, A., 1969. Palladium(II)-catalyzed oxidation of formic acid in acetic acid solution. J. Catal. 13, 283–289. https://doi.org/10.1016/0021-9517(69)90402-3.

Akhairi, M.A.F., Kamarudin, S.K., 2016. Catalysts in direct ethanol fuel cell (DEFC): an overview. Int. J. Hydrogen Energy. 41, 4214–4228. https://doi.org/10.1016/j.ijhydene.2015.12.145.

Al-Akraa, I.M., Mohammad, A.M., El-Deab, M.S., et al, 2015c. Advances in direct formic acid fuel cells: fabrication of efficient Ir/Pd nanocatalysts for formic acid electro-oxidation. Int. J. Electrochem. Sci. 10, 3282–3290. 10(2015)3282-3290.

Al-Akraa, I.M., Mohammad, A.M., El-Deab, M.S., et al, 2013. Self-assembling of gold nanoparticles array for electro-sensing applications. Int. J. Electrochem. Sci. 8, 458–466.

Al-Akraa, I.M., Mohammad, A.M., El-Deab, M.S., et al, 2015a. Electrocatalysis by design: Synergistic catalytic enhancement of formic acid electro-oxidation at core-shell Pd/Pt nanocatalysts. Int. J. Hydrogen Energy. 40, 1789–1794. https://doi.org/10.1016/j.ijhydene.2014.11.144.

Al-Akraa, I.M., Mohammad, A.M., El-Deab, M.S., et al, 2015b. Electrocatalysis by nanoparticle: Enhanced electro-oxidation of formic acid at NiOx-Pd binary nanocatalysts. J. Electrochem. Soc. 162, F1114–F1118. https://doi.org/10.1149/2.0151510jes.

Al-Akraa, I.M., Mohammad, A.M., El-Deab, M.S., et al, 2017. Flower-shaped gold nanoparticles: Preparation, characterization, and electrocatalytic application. Arab. J. Chem. 10, 877–884. https://doi.org/10.1016/j.arabjc.2015.05.004.

Al-Akraa, I.M., Salama, A.E., Asal, Y.M., et al, 2021. Boosted performance of NiOx/Pt nanocatalyst for the electro-oxidation of formic acid: a substrate's functionalization with multi-walled carbon nanotubes. Arab. J. Chem. 14. https://doi.org/10.1016/j.arabjc.2021.103383.

Al-Akraa, I.M., Mamdouh, M.M., Asal, Y.M., et al, 2022. A competent MWCNT-Grafted MnOx/Pt nanoanode for the direct formic acid fuel cells. J. Chem. 2022. https://doi.org/10.1155/2022/3762138.

Al-Akraa, I.M., Mohammad, A.M., 2020. A spin-coated TiOx/Pt nanolayered anodic catalyst for the direct formic acid fuel cells. Arab. J. Chem. 13, 4703–4711. https://doi.org/10.1016/j.arabjc.2019.10.013.

Al-Qodami, B.A., Farrag, H.H., Sayed, S.Y., et al, 2018. Bifunctional tailoring of platinum surfaces with earth abundant iron oxide nanowires for boosted formic acid electro-oxidation. J. Nanotechnol. 2018. https://doi.org/10.1155/2018/4657040.

Al-Qodami, B.A., Alalawy, H.H., Al-Akraa, I.M., et al, 2022a. Surface engineering of nanotubular ferric oxyhydroxide "goethite" on platinum anodes for durable formic acid fuel cells. Int. J. Hydrogen Energy. 47, 264–275. https://doi.org/10.1016/j.ijhydene.2021.10.037.

Al-Qodami, B.A., Alalawy, H.H., Sayed, S.Y., et al, 2022b. Tailor-designed nanowire-structured iron and nickel oxides on platinum catalyst for formic acid electro-oxidation. RSC Adv. 12, 20395–20402. https://doi.org/10.1039/d2ra03386k.

Anantharaj, S., Karthik, P.E., Noda, S., 2021. The Significance of Properly Reporting Turnover Frequency in Electrocatalysis Research. Angewandte Chemie – Int. Ed. 60, 23051–23067. https://doi.org/10.1002/anie.202110352.

Asal, Y.M., Mohammad, A.M., El Rehim, S.S.A., et al, 2021. Preparation of Co-electrodeposited Pd-Au Nanocatalyst for Methanol Electro-oxidation. Int. J. Electrochem. Sci. 16, 1–11. https://doi.org/10.20964/2021.11.30.

Asal, Y.M., Mohammad, A.M., Abd El Rehim, S.S., et al, 2022. Augmented formic acid electro-oxidation at a co-electrodeposited Pd/Au nanoparticle catalyst. J. Saudi Chem. Soc. 26. https://doi.org/10.1016/j.jscs.2022.101508.

Baik, S.M., Han, J., Kim, J., et al, 2011. Effect of deactivation and reactivation of palladium anode catalyst on performance of direct formic acid fuel cell (DFAFC). Int. J. Hydrogen Energy. 36, 14719–14724. https://doi.org/10.1016/j.ijhydene.2011.04.181.

Braunschweig, B., Hibbitts, D., Neurock, M., et al, 2013. Electrocatalysis: a direct alcohol fuel cell and surface science perspective. Catal. Today. 202, 197–209. https://doi.org/10.1016/j.cattod.2012.08.013.

Breiter, M.W., 1963. Anodic oxidation of formic acid on platinum—I. Adsorption of formic acid, oxygen, and hydrogen in perchloric acid solutions. Electrochim. Acta. 8, 447–456. https://doi.org/10.1016/0013-4686(63)85002-1.

Carmo, M., Doubek, G., Sekol, R.C., et al, 2013. Development and electrochemical studies of membrane electrode assemblies for polymer electrolyte alkaline fuel cells using FAA membrane and ionomer. J. Power Sources. 230, 169–175. https://doi.org/10.1016/j.jpowsour.2012.12.015.

Chang, J., Feng, L., Liu, C., et al, 2014. An effective Pd-Ni2P/C anode catalyst for direct formic acid fuel cells. Angewandte Chemie - International Edition. 53, 122–126. https://doi.org/10.1002/anie.201308620.

Choun, M., 2016. Investigation on formate oxidation on palladium and strategies for improving performance in alkaline direct formate fuel cells. Gwangju Institute of Science and Technology, South Korea. Doctoral Thesis.

Cui, Z., Yang, M., Disalvo, F.J., 2014. Mesoporous Ti0.5Cr0.5N supported PdAg nanoalloy as highly active and stable catalysts for the electro-oxidation of formic acid and methanol. ACS Nano 8, 6106–6113. https://doi.org/10.1021/nn5014337.

Doyle, R.L., Lyons, M.E.G., 2013. An electrochemical impedance study of the oxygen evolution reaction at hydrous iron oxide in base. Phys. Chem. Chem. Phys. 15, 5224–5237. https://doi.org/10.1039/c3cp43464h.

Egeland-Eriksen, T., Hajizadeh, A., Sartori, S., 2021. Hydrogen-based systems for integration of renewable energy in power systems: achievements and perspectives. Int. J. Hydrogen Energy. 46, 31963–31983. https://doi.org/10.1016/j.ijhydene.2021.06.218.

El-Deab, M.S., Mohammad, A.M., El-Nagar, G.A., et al, 2014. Impurities contributing to catalysis: enhanced electro-oxidation of formic acid at Pt/GC electrodes in the presence of vinyl acetate. J. Phys. Chem. C. 118, 22457–22464. https://doi.org/10.1021/jp507240r.

Elnabawy, A.O., Herron, J.A., Scaranto, J., et al, 2018. Structure sensitivity of formic acid electrooxidation on transition metal surfaces: a first-principles study. J. Electrochem. Soc. 165, J3109–J3121. https://doi.org/10.1149/2.0161815jes.

El-Nagar, G.A., Mohammad, A.M., El-Deab, M.S., et al, 2012. Facilitated electro-oxidation of formic acid at nickel oxide nanoparticles modified electrodes. J. Electrochem. Soc. 159, F249–F254. https://doi.org/10.1149/2.043207jes.

El-Nagar, G.A., Mohammad, A.M., El-Deab, M.S., et al, 2013. Electrocatalysis by design: Enhanced electrooxidation of formic acid at platinum nanoparticles-nickel oxide nanoparticles binary catalysts. Electrochim. Acta 94, 62–71. https://doi.org/10.1016/j.electacta.2013.01.133.

El-Nagar, G.A., El-Deab, M.S., Mohammad, A.M., et al, 2015. Promoting effect of hydrocarbon impurities on the electro-oxidation of formic acid at Pt nanoparticles modified GC electrodes. Electrochim. Acta. 180, 268–279. https://doi.org/10.1016/j.electacta.2015.08.119.

El-Nagar, G.A., Mohammad, A.M., El-Deab, M.S., et al, 2014a. Electro-oxidation of formic acid at binary platinum and gold nanoparticle-modified electrodes: effect of chloride ions. Int. J. Electrochem. Sci. 9, 4523–4534.

El-Nagar, G.A., Mohammad, A.M., El-Deab, M.S., et al., 2014. Electrocatalysis by nanoparticles: Oxidation of formic acid at novel Pt/NiOx nanoparticles-based binary catalysts. International Conference on Industry Academia Collaboration (IAC2014), Fairmont Hotel, Cairo, Egypt.

El-Nagar, G.A., Mohammad, A.M., El-Deab, M.S., et al, 2017. Propitious dendritic Cu_2O-Pt nanostructured anodes for direct formic acid fuel cells. ACS Appl. Mater. Interfaces. 9, 19766–19772. https://doi.org/10.1021/acsami.7b01565.

Eppinger, J., Huang, K.-W., 2017. Formic acid as a hydrogen energy carrier. ACS Energy Lett. 2, 188–195. https://doi.org/10.1021/acsenergylett.6b00574.

Faid, A.Y., Barnett, A.O., Seland, F., et al, 2019. Optimized nickel-cobalt and nickel-iron oxide catalysts for the hydrogen evolution reaction in alkaline water electrolysis. J. Electrochem. Soc. 166, F519–F533. https://doi.org/10.1149/2.0821908jes.

Ferrer, J.E., Victori, L., 1993. Electro-oxidation of formic acid on the iridium electrode as a function of pH. Electrochim. Acta. 38, 1631–1636. https://doi.org/10.1016/0013-4686(93)85052-Z.

Fu, J., Jiang, X., Han, W., et al, 2021. Enhancing the cycling stability of transition-metal-oxide-based electrochemical electrode via pourbaix diagram engineering. Energy Storage Mater. 42, 252–258. https://doi.org/10.1016/j.ensm.2021.07.037.

Haan, J.L., Stafford, K.M., Masel, R.I., 2010. Effects of the addition of antimony, Tin, and lead to palladium catalyst formulations for the direct formic acid fuel cell. J. Phys. Chem. C. 114, 11665–11672. https://doi.org/10.1021/jp102990t.

Han, S.D., Choi, J.H., Noh, S.Y., et al, 2009. Performance characterization of direct formic acid fuel cell using porous carbon-supported palladium anode catalysts. Korean J. Chem. Eng. 26, 1040–1046. https://doi.org/10.1007/s11814-009-0173-z.

Hong, P., Luo, F., Liao, S., et al, 2011. Effects of Pt/C, Pd/C and PdPt/C anode catalysts on the performance and stability of air breathing direct formic acid fuel cells. Int. J. Hydrogen Energy. 36, 8518–8524. https://doi.org/10.1016/j.ijhydene.2011.04.081.

Hoshi, N., Kida, K., Nakamura, M., et al, 2006. Structural effects of electrochemical oxidation of formic acid on single crystal electrodes of palladium. J. Phys. Chem. B. 110, 12480–12484. https://doi.org/10.1021/jp0608372.

Hu, S., Scudiero, L., Ha, S., 2012b. Electronic effect on oxidation of formic acid on supported Pd-Cu bimetallic surface. Electrochim. Acta. 83, 354–358. https://doi.org/10.1016/j.electacta.2012.06.111.

Hu, S., Scudiero, L., Ha, S., 2014. Electronic effect of Pd-transition metal bimetallic surfaces toward formic acid electrochemical oxidation. Electrochem. Commun. 38, 107–109. https://doi.org/10.1016/j.elecom.2013.11.010.

Hu, C., Ting, S.W., Chan, K.Y., et al, 2012a. Reaction pathways derived from DFT for understanding catalytic decomposition of formic acid into hydrogen on noble metals. Int. J. Hydrogen Energy. 37, 15956–15965. https://doi.org/10.1016/j.ijhydene.2012.08.035.

Jayashree, R.S., Spendelow, J.S., Yeom, J., et al, 2005. Characterization and application of electrodeposited Pt, Pt/Pd, and Pd catalyst structures for direct formic acid micro fuel cells. Electrochim. Acta. 50, 4674–4682. https://doi.org/10.1016/j.electacta.2005.02.018.

Larsen, R., Zakzeski, J., Masel, R.I., 2005. Unexpected activity of palladium on vanadia catalysts for formic acid electro-oxidation. Electrochem. Solid-State Lett. 8, A291–A293. https://doi.org/10.1149/1.1904464.

Lee, S.Y., Jung, N., Cho, J., et al, 2014. Surface-rearranged Pd3Au/C nanocatalysts by using CO-induced segregation for formic acid oxidation reactions. ACS Catal. 4, 2402–2408. https://doi.org/10.1021/cs500227j.

Li, R., Hao, H., Cai, W.B., et al, 2010. Preparation of carbon supported Pd-Pb hollow nanospheres and their electrocatalytic activities for formic acid oxidation. Electrochem. Commun. 12, 901–904. https://doi.org/10.1016/j.elecom.2010.04.016.

Liu, Y., Wang, L., Wang, G., et al, 2010. High Active Carbon Supported PdAu Catalyst for Formic Acid Electrooxidation and Study of the Kinetics. J. Phys. Chem. C. 114, 21417–21422. https://doi.org/10.1021/jp105779r.

Liu, Z., Zhang, X., 2009. Carbon-supported PdSn nanoparticles as catalysts for formic acid oxidation. Electrochem. Commun. 11, 1667–1670. https://doi.org/10.1016/j.elecom.2009.06.023.

Liu, Z., Zhang, X., Tay, S.W., 2012. Nanostructured PdRu/C catalysts for formic acid oxidation. J. Solid State Electrochem. 16, 545–550. https://doi.org/10.1007/s10008-011-1378-8.

Maji, A., Singh, O., Singh, S., et al, 2020. Palladium-Based Catalysts Supported by Unsymmetrical XYC–1 Type Pincer Ligands: C5 Arylation of Imidazoles and Synthesis of Octinoxate Utilizing the Mizoroki-Heck Reaction. Eur. J. Inorg. Chem. 2020, 1596–1611. https://doi.org/10.1002/ejic.202000211.

Mardini, N., Biçer, Y., 2021. Direct synthesis of formic acid as hydrogen carrier from CO_2 for cleaner power generation through direct formic acid fuel cell. Int. J. Hydrogen Energy. 46, 13050–13060.

Nishimura, S., Ikeda, N., Ebitani, K., 2014. Selective hydrogenation of biomass-derived 5-hydroxymethylfurfural (HMF) to 2,5-dimethyl-furan (DMF) under atmospheric hydrogen pressure over carbon supported PdAu bimetallic catalyst. Catal. Today. 232, 89–98. https://doi.org/10.1016/j.cattod.2013.10.012.

Oishi, K., Savadogo, O., 2013. Electrochemical investigation of Pd–Co thin films binary alloy for the oxygen reduction reaction in acid medium. J. Electroanal. Chem. 703, 108–116. https://doi.org/10.1016/j.jelechem.2013.04.006.

Orozco, G., Gutiérrez, C., 2000. Adsorption and electro-oxidation of carbon monoxide, methanol, ethanol and formic acid on osmium electrodeposited on glassy carbon. J. Electroanal. Chem. 484, 64–72. https://doi.org/10.1016/S0022-0728(00)00062-0.

Qian, W., Wilkinson, D.P., Shen, J., et al, 2006. Architecture for portable direct liquid fuel cells. J. Power Sources. 154, 202–213. https://doi.org/10.1016/j.jpowsour.2005.12.019.

Shen, L., Li, H., Lu, L., et al, 2013. Improvement and mechanism of electrocatalytic performance of Pd-Ni/C anodic catalyst in direct formic acid fuel cell. Electrochim. Acta. 89, 497–502. https://doi.org/10.1016/j.electacta.2012.10.077.

Shervedani, R.K., Bagherzadeh, M., 2008. Hydroxamation of gold surface via in-situ layer-by-layer functionalization of cysteamine self-assembled monolayer: Preparation and electrochemical characterization. Electrochim. Acta. 53, 6293–6303. https://doi.org/10.1016/j.electacta.2008.04.051.

Sneed, B.T., Young, A.P., Jalalpoor, D., et al, 2014. Shaped Pd-Ni-Pt core-sandwich-shell nanoparticles: Influence of Ni sandwich layers on catalytic electrooxidations. ACS Nano 8, 7239–7250. https://doi.org/10.1021/nn502259g.

Wang, Y., Qi, Y., Zhang, D., et al, 2014. New Insight into the Decomposition Mechanism of Formic Acid on Pd(111): Competing Formation of CO2 and CO. J. Phys. Chem. C 118, 2067–2076. https://doi.org/10.1021/jp410742p.

Wang, X., Xia, Y., 2008. Electrocatalytic performance of PdCo-C catalyst for formic acid oxidation. Electrochem. Commun. 10, 1644–1646. https://doi.org/10.1016/j.elecom.2008.08.043.

Wang, X., Hu, J.-M., Hsing, I.M., 2004. Electrochemical investigation of formic acid electro-oxidation and its crossover through a Nafion® membrane. J. Electroanal. Chem. 562, 73–80. https://doi.org/10.1016/j.jelechem.2003.08.010.

Wang, X., Tang, Y., Gao, Y., et al, 2008. Carbon-supported Pd-Ir catalyst as anodic catalyst in direct formic acid fuel cell. J. Power Sources. 175, 784–788. https://doi.org/10.1016/j.jpowsour.2007.10.011.

Wen, W., Li, C., Li, W., et al, 2013. Carbon-supported Pd–Cr electrocatalysts for the electrooxidation of formic acid that demonstrate high activity and stability. Electrochim. Acta. 109, 201–206. https://doi.org/10.1016/j.electacta.2013.07.137.

Xiang, J., Wu, B.-L., Chen, S.-L., 2001. Investigation of the mechanism of the electrochemical oxidation of formic acid at a gold electrode in sulfuric acid solution. J. Electroanal. Chem. 517, 95–100. https://doi.org/10.1016/S0022-0728(01)00680-5.

Ye, W., Chen, S., Ye, M., et al, 2017. Pt4PdCu0.4 alloy nanoframes as highly efficient and robust bifunctional electrocatalysts for oxygen reduction reaction and formic acid oxidation. Nano Energy 39, 532–538. https://doi.org/10.1016/j.nanoen.2017.07.025.

Yu, X., Pickup, P.G., 2008. Recent advances in direct formic acid fuel cells (DFAFC). J. Power Sources 182, 124–132. https://doi.org/10.1016/j.jpowsour.2008.03.075.

Yuan, D.W., Liu, Z.R., 2013. Atomic ensemble effects on formic acid oxidation on PdAu electrode studied by first-principles calculations. J. Power Sources. 224, 241–249. https://doi.org/10.1016/j.jpowsour.2012.09.113.

Zhang, J. (Ed.), 2008. PEM Fuel Cell ElectroCatalysts and Catalyst Layers: Fundamentals and Applications. Springer, London.

Zhang, R., Liu, H., Wang, B., et al, 2012. Insights into the preference of CO_2 formation from HCOOH decomposition on Pd surface: a theoretical study. J. Phys. Chem. C 116, 22266–22280. https://doi.org/10.1021/jp211900z.

Zhang, S., Shao, Y., Yin, G., et al, 2010. Facile synthesis of PtAu alloy nanoparticles with high activity for formic acid oxidation. J. Power Sources. 195, 1103–1106. https://doi.org/10.1016/j.jpowsour.2009.08.054.